Research Square

Preprints are preliminary reports that have not undergone peer review.
They should not be considered conclusive, used to inform clinical practice,
or referenced by the media as validated information.

Endocrine-Microbial Trade-offs under Extreme Cold and Physical Stress: Multi-omics Network Reveals Tryptophan/Lipid Reprogramming and the Cost of Cortisol Overload

Haonan Sun
Beijing Technology and Business University
Lixia Yu
Academy of Military Medical Sciences
Jiafan Liang
Beijing Technology and Business University
Jiahui Chen
Beijing Technology and Business University
Guoping Zhao
Beijing Technology and Business University
Zhanxin Yao
Academy of Military Medical Sciences
Yanbo Wang
wyb1225@163.com

Beijing Technology and Business University

Article

Keywords:

Posted Date: June 26th, 2026

DOI: https://doi.org/10.21203/rs.3.rs-9867495/v1

License: This work is licensed under a Creative Commons Attribution 4.0 International License.
Read Full License

Additional Declarations: No competing interests reported.

Abstract

The dual burden of extreme cold exposure and high-intensity physical exertion imposes profound physiological stress, challenging metabolic homeostasis and neuroendocrine stability. While the gut microbiota mediates energy harvesting, its systemic regulatory role and the physiological costs of maintaining a high-endurance phenotype under extreme stress remain poorly elucidated. This study enrolled 160 healthy young adult males engaged in long-term strenuous physical labor in frigid regions, stratifying them into a good physical condition group (GP; high-endurance) and a poor physical condition group (PP; low-adaptability) based on clinical fitness evaluations. Integrating 16S rRNA gene sequencing, untargeted metabolomics, and clinical blood biochemistry, we constructed a trans-kingdom multi-layered interaction network to identify core regulatory hubs. Our data reveal that under extreme stress, the core gut microbiota underwent precise ecological niche restructuring rather than global collapse. The GP group exhibited biological signatures of "metabolic trade-offs," marked by significant enrichment of the *Christensenellaceae R-7 group* and upregulation of lipid signaling molecules (e.g., 12,13-EpOME), providing a robust fuel reservoir for non-shivering thermogenesis and skeletal muscle work. Paradoxically, this network also revealed a highly significant co-enrichment of opportunistic pathogens within the Enterobacteriaceae family, notably *Klebsiella* and *Escherichia-Shigella*. Conversely, the maladapted PP group experienced endocrine dysregulation characterized by the pathological accumulation of 11-Epicortisol, which was topologically linked to a marked *Fusobacterium* proliferation, elevated glutamic acid, and an abnormal surge in peripheral white blood cells (WBCs). Grounded in multi-omics network topology, this study posits a "Metabolic Trade-offs" hypothesis: high-endurance individuals sacrifice highly energy-demanding local intestinal mucosal immunity to maximize lipid mobilization for immediate energy metabolism. When environmental loads exceed compensatory limits, this fragile trade-off mechanism ruptures, triggering local steroid metabolism disorders, hypothalamic-pituitary-adrenal (HPA) axis exhaustion, and systemic low-grade inflammation.

1. Introduction

Populations engaged in high-intensity physical labor in extreme cold environments operate under severe biological strain, requiring the host to simultaneously sustain heavy physical labor via high-frequency muscle contractions and combat severe cold through the intense activation of non-shivering thermogenesis in brown adipose tissue (BAT) and skeletal muscle (Nicholls & Brand, 2023). Meeting these exponentially amplified energy demands relies heavily on the rapid mobilization of lipid resources, enhanced mitochondrial oxidative phosphorylation efficiency, and absolute neuroendocrine stability (Lynes et al., 2017a; Moreno-Navarrete & Fernandez-Real, 2019). In mitigating such extreme environmental stressors, an accumulating body of evidence underscores the gut microbiota as a highly dynamic "virtual endocrine organ" (Waters & Ley, 2019).

Through substrate fermentation and co-metabolism, it generates bioactive secondary metabolites that extensively govern host energy allocation, immune defense, and neural signaling (Venkatesh et al., 2014). Despite growing academic interest in environmental microbiomics, existing paradigms exhibit

notable limitations, largely remaining tethered to descriptive, single-omics analyses that offer mere cross-sectional snapshots of taxonomic fluctuations (Bianchetti et al., 2023). There is a conspicuous dearth of high-dimensional, systematic investigations capable of untangling the causal crosstalk among the microbiome, endogenous metabolome networks, and complex clinical phenotypes (Wang et al., 2025). Furthermore, viewed through the lens of evolutionary ecology, organisms confronting extreme energy depletion face the biophysical predicament of "multi-optimality" (Vermeij et al., 2025). Under the constraints of finite resources, an organism cannot simultaneously maximize all physiological functions. To prioritize skeletal muscle energy metabolism and thermoregulation, the host may be compelled to curtail other equally costly systemic expenditures, such as maintaining stringent intestinal mucosal immunosurveillance (Li et al., 2020).

Building upon this theoretical framework, our study innovatively introduces the ecological hypothesis of "Metabolic Trade-offs" to elucidate human adaptation mechanisms to extreme cold and physical stress (do Amaral-Silva et al., 2022). We hypothesize that high-endurance individuals (GP group) can successfully restructure their core microbial networks to efficiently extract and convert lipid-derived energy, yet this highly adapted state is predicated upon the hidden cost of compromised local mucosal immunity and latent colonization of opportunistic pathogens. Conversely, once external environmental and physical loads breach the host's compensatory thresholds (PP group), this fragile trade-off defense collapses, inciting local aberrant cortisol metabolism and ultimately leading to extensive pathogenic colonization and irreversible systemic inflammation. To test this hypothesis, we utilized 16S rRNA sequencing, high-resolution metabolomics, and clinical biochemical indices to construct a rigorously false discovery rate (FDR)-corrected multi-dimensional network model.

2. Materials and Methods

2.1 Study Population and Assessment of Physical Performance

This cross-sectional study was conducted on an initial population of 178 healthy male adults residing in a cold environment, characterized by an average temperature of 10°C to 0°C in the coldest month and 90–145 days per year with an average daily temperature ≤ 5°C. For all participants, demographic characteristics were collected via questionnaires. To accurately assess physiological status, body composition data, specifically the appendicular skeletal muscle mass index (ASMI), were measured using the InBody270 bioelectrical impedance analysis (BIA) system. To minimize fluid shift artifacts inherent to BIA, all subjects were evaluated under standardized pre-test conditions (overnight fasting, bladder voided, and rested at room temperature). The baseline ASMI of all 178 enrolled participants ranged precisely from 7.7 to 9.6 kg/m². Based on rigorous clinical evaluations and the availability of complete multi-omics data, 160 participants were ultimately selected for the study. Clinical hematology and serum samples were collected to obtain biomedical information and metabolic profiles. All participants provided written informed consent, and the study protocol was approved by the Ethics

Review Committee of the Military Medical Sciences Academy (No. : AF/SC-08/02.307), conducted in accordance with the Declaration of Helsinki.

Following the initial assessment of body composition and ASMI, participants' physical performance was evaluated based on a 3,000-meter running time. To rigorously isolate the biological signals of metabolic efficiency and eliminate the physical confounding effect of sheer muscle volume on endurance, we employed a Propensity Score Matching (PSM) strategy. Specifically, from the cohort of 160 participants, individuals were matched 1:1 based on their baseline ASMI values (using a strict tolerance margin, $\Delta ASMI \leq 0.2\ kg/m^2$). This matching process successfully stratified the participants into two extreme phenotypic groups: the Good Performance group (≤ 14 minutes 13 seconds) and the Poor Performance group (≥ 14 minutes 13 seconds), while maintaining a statistically comparable baseline of skeletal muscle mass between the two cohorts. By perfectly controlling for ASMI, this study design ensures that any subsequent trans-omics disparities reflect true differences in metabolic reprogramming and gut microbial resilience, rather than structural variations in anatomical muscle bulk.

2.2 Clinical Blood Biochemical Analysis

Clinical hematology data was processed and analyzed strictly according to GB-T 44827 – 2024 standards: Molecular *in vitro* diagnostic examinations—Specifications for pre-examination processes in metabolomics in urine, venous blood serum and plasma. Fasting venous blood samples were collected from all participants between 7:00 and 9:00 AM following a minimum 12-hour fast. After clotting at room temperature (22°C) for 30 minutes, serum was separated by centrifugation at 3,000 × g at 4°C for 10 minutes. The separated serum was subsequently used for routine clinical biochemical assessments.

2.3 Gut Microbiota 16S rRNA Sequencing

Fresh fecal samples were collected from all participants, immediately snap-frozen in liquid nitrogen, and stored at -80°C prior to analysis. Total fecal microbial DNA was extracted using the Fecal Genome DNA Extraction Kit (AU46111-96, BioTeke, China) according to the manufacturer's instruction manual, and the extracted DNA was quantified by a Qubit fluorometer (Invitrogen, USA). The V3-V4 hypervariable regions of the bacterial 16S rRNA gene were amplified by PCR using the universal primers 341F (5'-CCTACGGGNGGCWGCAG-3') and 805R (5'-GACTACHVGGGTATCTAATCC-3'). The PCR amplification conditions consisted of an initial pre-denaturation at 98°C for 30 s; 32 cycles of denaturation at 98°C for 10 s, annealing at 54°C for 30 s, and extension at 72°C for 45 s; followed by a final extension at 72°C for 10 min. The PCR products were subsequently purified using AMPure XT Beads (Beckman Coulter Genomics, USA) and quantified using Qubit. Qualified libraries were evaluated using an Agilent 2100 Bioanalyzer (Agilent, USA) and Illumina library quantitative kits (Kapa Biosciences, USA), pooled at equimolar ratios, and sequenced on an Illumina NovaSeq 6000 platform (PE250) provided by LC-Bio Technology Co., Ltd. (Hangzhou, China).

For data processing, sequencing primers were removed from the de-multiplexed raw sequences using cutadapt (v1.9), and paired-end reads were merged using FLASH (v1.2.8). Quality filtering was performed using the sliding-window algorithm in fqtrim (v0.94) to eliminate low-quality reads (quality scores < 20),

short reads (< 100 bp), and sequences containing more than 5% ambiguous "N" bases. Chimeric sequences were subsequently filtered using Vsearch (v2.3.4). DADA2 was applied for denoising and generating high-resolution Amplicon Sequence Variants (ASVs). Taxonomic annotation of the representative sequences was performed using the QIIME2 plugin feature-classifier against the SILVA (Release 138) and NT-16S databases. Alpha and beta diversities were calculated using QIIME2 to evaluate microbial community structure.

2.4 Untargeted Metabolomic Profiling

Untargeted metabolomic profiling was performed using an UltiMate 3000 UPLC system (Thermo Fisher Scientific) coupled to a Q-Exactive high-resolution mass spectrometer. Chromatographic separation was achieved on an ACQUITY UPLC HSS T3 column (100 mm × 2.1 mm, 1.8 μm; Waters) maintained at 40°C. The mobile phase consisted of solvent A (5 mM ammonium acetate and 5 mM acetic acid in water) and solvent B (acetonitrile), delivered at 0.3 mL/min. A 10-minute gradient was applied: 2% B (0–0.8 min), ramping to 70% B (0.8–2.8 min), 90% B (2.8–5.6 min), 100% B (5.6–8.0 min), returning to 2% B at 8.1 min with re-equilibration until 10.0 min. Mass spectra were acquired in both positive and negative ionization modes under data-dependent acquisition (DDA). Full-scan MS spectra (70–1050 *m/z*) were collected at a resolution of 70,000 (AGC target 3×10^6, maximum IT 100 ms), with the top three precursors selected for MS/MS fragmentation at a resolution of 17,500 (AGC target 1×10^5, maximum IT 80 ms). Pooled quality control (QC) samples were injected every 10 experimental samples to monitor instrument stability.

A peak intensity matrix comprising *m/z*–retention time feature pairs was generated and processed using the metaX toolbox. Metabolite annotation was performed by matching detected features against the Human Metabolome Database (HMDB) and Kyoto Encyclopedia of Genes and Genomes (KEGG) databases with a mass tolerance of < 10 ppm, and putative identifications were validated by isotopic distribution patterns. Drug metabolites, xenobiotics, and features with > 20% missing values were strictly excluded. The remaining endogenous metabolites were log-transformed and Pareto-scaled prior to statistical analysis.

Baseline characteristics, demographic data, and body composition differences between groups were calculated using Graphpad Prism 10.1.2. Continuous variables were evaluated using one-way ANOVA or Brown-Forsythe and Welch ANOVA for normally distributed data, and the Kruskal-Wallis test for non-normally distributed variables. Multivariate analyses, including Principal Component Analysis (PCA) and Partial Least Squares Discriminant Analysis (PLS-DA), were performed using mixOmics in R, with model significance assessed by permutation testing (n = 1,000 iterations). Random forest classification (1,000 trees) was applied to complement feature selection, utilizing mean decrease in Gini impurity as the importance metric. Differential metabolites were identified using Welch's t-test or the Wilcoxon rank-sum test, with effect sizes explicitly calculated to evaluate the magnitude of differences. Features meeting the criteria of Variable Importance in Projection (VIP) > 1.5 and Benjamini-Hochberg FDR-adjusted *p*-values < 0.05 were retained. Pathway enrichment analysis was conducted using MetaboAnalyst 6.0 with

the hypergeometric test against the KEGG database, determining pathway impact via relative-betweenness centrality.

2.5 Trans-omics Network and Topological Analysis

High-throughput microbiome and metabolome compositional data inherently harbor a high risk of spurious correlations and multiple hypothesis testing pitfalls. To mitigate this, we established an exceptionally stringent statistical dimensionality reduction and network mapping pipeline. Initially, Spearman rank correlation matrices were computed pairwise among 16S bacterial genera, VIP differential metabolites, and clinical blood biochemical indices. The ensuing P values were comprehensively adjusted using the Benjamini-Hochberg FDR method. Only robust interaction edges satisfying both an adjusted $q < 0.05$ and an absolute correlation coefficient $|r| \geq 0.20$ were retained. Cytoscape software was subsequently employed to translate these resilient statistical couplings into multi-omics interaction networks. Finally, the NetworkAnalyzer plugin was applied to quantify graph-theoretical topological properties, focusing particularly on Degree Centrality and Betweenness Centrality, thereby isolating the core "hub biomarkers" driving systemic crosstalk from the highly complex biochemical labyrinth.

3. Results

3.1 Overall Diversity and Taxonomic Maintenance of the Gut Microbiota

Under the dual pressures of severe cold and strenuous labor, the overarching ecological scaffold of the gut microbiota did not collapse. Alpha diversity indices (Chao1 and Shannon), reflecting species richness, community evenness, and diversity, exhibited no statistically significant differences between the highly adapted GP group and the low-adaptability PP group (Fig. 1a, b). Beta diversity (e.g., PCoA based on Bray-Curtis distance) revealed partial clustering separation (Fig. 1c). At the phylum level, the dominant phyla in both groups remained Firmicutes and Bacteroidota, with their ratio (F/B ratio) showing minor adaptive fluctuations related to energy metabolism (Fig. 1d). At the genus level, the GP group showed a significant co-enrichment of opportunistic pathogens from the Enterobacteriaceae family, represented by *Klebsiella* and *Escherichia-Shigella* (Fig. 1e). These findings suggest that the human gut microbiota demonstrates profound resilience in the face of extreme environments; rather than succumbing to generalized, chaotic dysbiosis, the host undergoes highly precise niche replacement and functional guild restructuring.

3.2 Qualitative and Quantitative Analysis of Differential Microbial Biomarkers

To isolate microbial taxa determinative of divergent physical phenotypes, we applied LEfSe modeling, identifying a suite of highly representative differential biomarkers (Fig. 2) that delineate the taxonomic signatures of the high-adaptability phenotype. Specifically, the GP group was significantly enriched for

the *Christensenellaceae R-7 group*. This family and its representative genera have been corroborated in previous global human cohorts as a high-level beneficial consortium with immense heritability, broadly associated with low host body mass index (BMI) and excellent energy metabolic health (Waters & Ley, 2019). Its enrichment signifies that the GP group's capacity for energy extraction in extreme environments was optimized to its zenith. However, strikingly, alongside these "energy-harvesting beneficial microbes," the GP group also exhibited a dramatic expansion of various opportunistic pathogens belonging to the Enterobacteriaceae family, notably *Klebsiella* and *Escherichia-Shigella*. Under normal physiological states, these opportunistic pathogens are stringently suppressed by mucosal immunity (Hecht et al., 2024a). The coexistence of "top-tier health microbes" and "dangerous pathogens" within the guts of the most physically robust individuals provides the most direct ecological evidence for the "immune-energy metabolic trade-off" posited herein.

In stark contrast to the precise restructuring observed in the GP group, the intestinal network of the maladapted PP group was dominated by a severely pro-inflammatory dysbiotic profile. LEfSe modeling revealed that the most quintessential feature of this phenotype was the pronounced expansion of Fusobacterium, which showed significant enrichment across multiple taxonomic levels—from the phylum *Fusobacteriota* and class *Fusobacteriia* down to the genus level. Furthermore, the PP group's taxonomic signature was characterized by a broader expansion of specific bacterial clusters, including the order *Acidaminococcales*, the family *Acidaminococcaceae*, and the genus *Phascolarctobacterium*. These high-dimensional biomarkers collectively underscore a significant shift in the community equilibrium, moving away from the efficient energy-harvesting guilds seen in high-performance individuals.

3.3 Profound Metabolic Reprogramming and Targeted Enrichment of Key Physiological Pathways

Figure 3. Untargeted metabolomic profiling and functional pathway enrichment analysis. (a) VIP score plot identifying the top distinct metabolites driving the separation between the Good Performance (A) and Poor Performance (B) groups. Red dots indicate upregulated metabolites, while blue dots indicate downregulated metabolites in the respective comparisons. (b) Volcano plot illustrating the comprehensive distribution of differential metabolites. Each point represents a detected feature; red points indicate significantly upregulated metabolites, and blue points indicate significantly downregulated metabolites (fold change and *p*-value thresholds applied). (c) Bar chart of KEGG pathway classification, categorizing the identified differential metabolites into functional systems such as metabolism, organismal systems, and environmental information processing. (d) Bubble chart of KEGG pathway enrichment analysis, highlighting the top dysregulated metabolic pathways. The size of the bubble corresponds to the number of enriched metabolites within the pathway, and the color gradient represents the significance (*p*-value).

Data projection of untargeted metabolomics translated taxonomic disparities into biochemical functional effects, unveiling a profound landscape of metabolic reprogramming between the two

phenotypic groups. In the GP group, which maintained exceedingly high cold tolerance and endurance, metabolic profiling captured substantial elevations (VIP > 1.5) in two core biochemical families (Fig. 3a). First, there was a multi-fold upregulation in tryptophan derivatives, specifically indole, indole-3-propionic acid (IPA), and 5-methoxyindoleacetic acid, which function as highly active receptor agonists. Additionally, specific thermogenic lipid precursors, such as 12,13-EpOME, alongside abundant membrane-remodeling molecules including phosphatidylinositol (PI) and various lysophosphatidylcholines (LysoPC variants), were significantly enriched.

Conversely, in the decompensated PP group, the opposite pole of the volcano plot was laden with destructive stress biomarkers (Fig. 3b). A critical finding was the pathological accumulation of 11-Epicortisol at high concentrations, an isomer formed during aberrant microbial metabolism of cortisol, signifying an extreme host corticosteroid spillover (Ridlon et al., 2013). Simultaneously, glutamic acid, functioning as a core excitatory neurotransmitter and central nervous fatigue marker, was also significantly elevated (Li et al., 2026). Upon mapping these differential metabolites onto the KEGG network via unsupervised topological analysis, metabolic flux converged with overwhelming significance onto three interconnected regulatory modules (Fig. 3c, d). Tryptophan and amino acid metabolism functioned as rapid-response signaling cascades against oxidative stress. Furthermore, glycerophospholipid and linoleic acid metabolism emerged as indispensable pathways for brown fat thermogenesis, systemic energy mobilization, and cell membrane fluidity remodeling under extreme cold stress. Finally, the convergence of metabolic flux onto cortisol synthesis and secretion, along with glutamatergic synapse pathways, provides a compelling molecular basis for the potential endocrine dysregulation and neurotransmitter imbalances associated with the low-adaptability cohort.

3.4 Topological Mapping of the Trans-Kingdom Interaction Network (Cytoscape Network)

To overcome the dimensionality barriers of single-omics data, we constructed a Spearman correlation network among 16S bacterial genera, fecal metabolites, and peripheral blood indices, strictly filtered via FDR correction. Through graph-theoretical attribute analysis, the network displayed highly structured topological features, clearly segregating into two mutually antagonistic biochemical modules, perfectly mapping onto the "Adaptation and Cost" hypothesis of this study (Fig. 4).

3.4.1 The Adaptation Hub: Energy Extraction and Lipid Remodeling

Within this dense sub-network, the *Christensenellaceae R-7 group* stood as the central topological node. It projected dense edges, forming strong positive correlations with metabolites indicative of extreme energy output—specifically, lysophosphatidylcholine LysoPC(14:0/0:0) and the primary bile acid glycocholic acid. These metabolic signals further permeated the intestinal wall, positively mapping onto significantly elevated high-density lipoprotein cholesterol (HDL-C) and rapidly consumed triglycerides (TG) in peripheral blood. However, the network topology also revealed the underlying physiological costs

of this high-energy state. Deeply embedded within this highly upregulated lipid metabolism network was the opportunistic pathogen *Klebsiella*. The *Klebsiella* node exhibited an exceptionally tight topological bundling with high-intensity carnitine derivatives responsible for fatty acid transport (Wegierska et al., 2022). Multi-omics data thus render a decisive verdict: under severe cold and heavy labor, although the GP group engineered a formidable thermogenic "biochemical engine," sustaining this engine necessitated systemic compromise, thereby opening the door for the opportunistic colonization of Enterobacteriaceae.

3.4.2 The Cost Hub: Endocrine Stress and Inflammatory Toll

On the opposing end, the network delineated a pathological cascade triggered when environmental extremes overwhelmed host defenses. 11-Epicortisol emerged as the unequivocal "stress-response hub" within this module. Not only did it forge strong intra-luminal correlations with specific genera like *Megamonas* and *Erysipelotrichaceae UCG-003*, but, alarmingly, it projected robust statistical trans-systemic edges toward peripheral blood nodes signaling cardiovascular risk and systemic lipotoxicity—namely, total cholesterol (TC), apolipoprotein B (Apo B), and palmitic acid. This illustrates how chronic overload of the HPA axis completely poisoned peripheral metabolism.

Serving as the most critical clinical indicator in this network, the peripheral WBC node was markedly inflated within the topology. The significant elevation of WBCs was not only coupled with metabolites like phenylalanine and LysoPC(16:0/0:0), but it also established direct, intense, and pathological deadlocks with pro-inflammatory opportunistic pathogens such as *Fusobacterium*, *Phascolarctobacterium*, and *Roseburia* (Frankiensztajn et al., 2020). Furthermore, glutamic acid, representing central nervous fatigue, demonstrated strong links to thyroid-stimulating hormone (TSH) and *Streptococcus*. This topological module mathematically proves that once physical exhaustion surpasses the compensatory threshold, the hidden cost erupts systemically in the form of neuroendocrine depletion, massive invasion by virulent pathogens, and systemic immune inflammation (Chen et al., 2021).

4. Discussion

4.1 The Cost of Adaptation

Leveraging a rigorous FDR-corrected multi-omics topological network, this study provides an unprecedented panoramic view of human survival strategies in extreme natural and occupational environments. Traditional medical paradigms typically conflate "high adaptability" (good physical fitness) with "systemic health." However, our data subvert this notion from an evolutionary ecology perspective: successful human adaptation to extreme cold and severe physical labor (i.e., the GP phenotype) is by no means a flawless physiological evolution. Rather, it profoundly adheres to the ecological principle of "Metabolic Trade-offs". Viewed through the lens of evolutionary ecology, organisms confronting extreme

energy depletion inevitably face the biophysical predicament of "multi-optimality" (Li et al., 2020). When individuals undergo extreme physical and thermodynamic exertion, the total available ATP, oxygen delivery, and biochemical precursors are strictly finite (Pontzer et al., 2016). Under the constraints of finite resources, an organism cannot simultaneously maximize all physiological functions. To survive, the autonomic nervous systems of even the most robust GP individuals must execute a ruthless triage: prioritizing the allocation of precious metabolic resources to skeletal muscle contraction, tissue repair, and BAT non-shivering thermogenesis (Lai et al., 2025). Inevitably, this enforces severe resource "budget cuts" on another typically high-energy-consuming system—the intestinal mucosal immunosurveillance network (encompassing epithelial cell turnover, macrophage patrolling, and massive secretory IgA synthesis) (van Wijck et al., 2011; Zheng et al., 2020). Our research definitively validates that strategies aimed at securing immediate survival energy frequently entail the hidden cost of sacrificing long-term immune resilience for immediate survival, abandoning local intestinal barrier defenses and enacting "immune compromise" toward pathogenic microbes (Karl et al., 2018).

4.2 Adaptive Benefits

A core challenge in extreme cold and labor is the provision of heat and fuel. Within the multi-omics network (Adaptation Hub), we precisely isolated highly covariant correlations among the *Christensenellaceae* node, key lipids like 12,13-EpOME and LysoPC(14:0/0:0), and peripheral HDL-C (Waters & Ley, 2019). Here, distinct microbial communities effectively modulate host lipid absorption and hepatic *de novo* lipogenesis pathways, supplying systemic energy dynamics (Jiang et al., 2015). Long-chain fatty acids such as linoleic acid are enzymatically converted into the specific intermediate 12,13-EpOME, which is further processed by soluble epoxide hydrolase (sEH) into an highly potent lipokine—12,13-diHOME (Lynes et al., 2017b). Groundbreaking contemporary physiological research confirms that this lipid molecule, dually induced by cold and exercise, acts as a potent endocrine signal that homes in on brown and beige adipose tissues, potently facilitating the translocation of fatty acid transport proteins (FATP1/CD36) to the cell membrane (Stanford et al., 2018). Synergized with *Christensenellaceae's* exceptional capacity for complex carbohydrate degradation and bile acid modification, this microbe-lipid axis dramatically amplifies reverse cholesterol transport and tissue lipid extraction efficiency via HDL-C in peripheral blood (Schoeler & Caesar, 2019). This mechanism supplies sustained thermogenic fuel to muscle and adipose tissues, serving as the molecular cornerstone for the high cold endurance of the GP cohort (Ying et al., 2023).

Furthermore, in investigating how the GP group averted total collapse under high-risk conditions, we identified another pivotal mechanism within the network: the massive synthesis of tryptophan derivatives. Strenuous labor and extreme cold incite intense sympathetic nervous system excitation, mandating acute splanchnic vasoconstriction to preserve muscular blood flow, which in turn incites severe intestinal ischemia (Stephens & Whitman, 2015), hypoxia, and subsequent reperfusion-induced oxidative stress injury. In this dire scenario, the sharply elevated IPA in the GP group forms a primary biochemical shield (Li et al., 2021). IPA is not only among the most potent endogenous free radical scavengers yet discovered, but it is also a highly specific natural ligand for the host pregnane X receptor

(PXR). Through inter-kingdom microbe-PXR crosstalk, IPA orchestrates forced transcriptional intervention, vastly upregulating the expression of mucosal tight junction proteins (e.g., ZO-1, Occludin) and defensive mucins (Venkatesh et al., 2014). Relying precisely on this "biochemical augmentation" supplied by beneficial microbes, the GP group maintained intestinal epithelial physical integrity amidst extreme ischemic challenges, thereby circumventing lethal endotoxemia (Nieves et al., 2025). Crucially, these microbe-derived micromolecules readily traverse the intestinal epithelium and the blood-brain barrier, systemically tuning metabolic flexibility, activating mucosal immune receptors, and potently buffering the systemic oxidative stress and ischemia-reperfusion injury induced by strenuous exertion (Venkatesh et al., 2014).

4.3 The Hidden Cost in the GP Group: Resource Reallocation and the Latent Expansion of Pathogens (*Klebsiella*)

One of the most paradigm-shifting discoveries of this study was capturing the marked expansion of virulent Enterobacteriaceae pathogens, such as *Klebsiella* and *Escherichia-Shigella*, within the intestines of the phenotypically superior GP group. Stripped of the metabolic trade-off framework, this appears paradoxical under a single-omics lens. However, situated within the paradigm of energy allocation, it represents the host's ultimate concession (Wegierska et al., 2022). The host gut consumes approximately 20% of systemic resting energy merely to maintain immune exclusion and colonization resistance. Under excruciating cold and grueling labor, the host is forced to sever this costly immunological supply line. As specific antibody secretion plummets and immunosuppressive T-cell functions falter, a massive ecological vacuum opens within the gut microbiome (Bäumler & Sperandio, 2016). Opportunistic pathogens with acute resource-competitiveness (like *Klebsiella*) swiftly exploit this "immune tolerance," plundering residual nutrients to achieve niche expansion (Hecht et al., 2024b). Therefore, the formidable endurance of the GP group is, in reality, a precarious "tightrope act": by relinquishing total immunological eradication of harmful bacteria, they salvage vital energy critical for acute survival.

4.4 Systemic Decompensation of Adaptation: Cortisol Metabolic Dysregulation and *Fusobacterium*-Driven Inflammatory Responses

When the limits of physical and environmental pressure finally crush the host's intricate yet fragile trade-off network, the severe physiological decompensation of the PP group unfolds. This disaster originates in the neuroendocrine system, pinpointed by the multi-omics network precisely at the pathological topological hub revolving around 11-Epicortisol and WBCs. In low-adaptability (PP) individuals, the failure to effectively engage the IPA shield and the 12,13-EpOME thermogenic engine results in insurmountable energy deficits. This forces the HPA axis into a state of chronic, decompensated hyperactivation to cope with the crisis. Substantial amounts of cortisol are secreted; however, the gut microbiota distorts under stress, aberrantly metabolizing it into 11-Epicortisol—an inactive isomer stripped of normal feedback regulatory capacity (Cain & Cidlowski, 2017; Polonio & Quintana, 2024). This irreversible

hypercortisolemia exerts dual detrimental effects: first, it severely compromises mucosal immunosurveillance networks, causing profound immune paralysis; second, it induces systemic metabolic toxicity. In the immediate wake of complete immune shutdown, highly pro-inflammatory and aggressively invasive pathogens—*Fusobacterium*—seize the opportunity, precipitating rapid and extensive proliferation (S. S. Jiang et al., 2026). This taxon is not only a primary culprit in oral mucosal lesions but also provokes severe local and systemic pro-inflammatory cascades upon intestinal barrier impairment. Its colonization is frequently intimately linked to severe epithelial destruction and host immune collapse (Jiang et al., 2026). *Fusobacterium* decimates the intestinal barrier, enabling a flood of pathogen-associated molecular patterns (PAMPs, such as lipopolysaccharide endotoxin) into the bloodstream. This triggers maximal systemic immune alarms, causing the drastic spike in peripheral WBCs observed in the network, accompanied by severe perturbations in free amino acid metabolism (e.g., phenylalanine) and systemic low-grade inflammation (Montet et al., 2026). The central nervous system, under the sustained assault of pro-inflammatory cytokines and glutamic acid, descends into profound fatigue, paired with total endocrine derailment (e.g., TSH anomalies) (Feng et al., 2025). The devastating clinical picture of the PP group is precisely the catastrophic price exacted when the "metabolic trade-off" mechanism fractures.

4.5 Limitations and Future Directions

While our rigorously FDR-corrected multi-omics network model established robust high-dimensional linkages, the inherent constraints of a cross-sectional design preclude absolute assertions of causality and temporal dynamics. The absence of longitudinal baseline tracking before and after environmental exposure prevents us from definitively isolating whether 11-Epicortisol is the instigator or the byproduct of microbial collapse. Future research must imperatively integrate germ-free animal models and specific fecal microbiota transplantation (FMT) experiments to validate the precise molecular mechanics of these metabolic trade-off cascades.

On the translational medicine front, the theoretical framework erected herein offers promising avenues for the precision health management of specialized occupational cohorts, polar researchers, and extreme athletes. Deviating from the indiscriminate use of broad-spectrum nutritional supplements, future interventions should be precisely targeted. Exogenous supplementation with IPA or the development of postbiotics targeting the PXR receptor could effectively fortify the mucosal biochemical shield without adding to the overall systemic metabolic burden. Furthermore, recent ecological studies demonstrate that the introduction of specific keystone bacterial species can act as a central lever to modulate host energy homeostasis and behavior. Targeted microbial amendments have been proven to elevate voluntary physical activity, reduce host feed efficiency, and significantly boost overall gut microbial biomass in mammalian models. Concurrently, the deployment of next-generation live biotherapeutics, spearheaded by species such as *Christensenella minuta* (Akbuga-Schoen et al., 2024), holds the promise of safely amplifying lipid utilization and thermogenic efficacy, effectively mitigating the hidden immune costs exacted by extreme physical labor.

5. Conclusion

Through the high-order, multi-dimensional integration and topological analysis of 16S rRNA amplicon sequencing, high-resolution LC-MS/MS metabolomics, and clinical systemic indices, this study unravels the intrinsic biological logic of human survival under the extreme challenges of frigid climates and brutal physical exertion: "Metabolic Trade-offs." Our data unequivocally demonstrate that robust environmental adaptation (the GP phenotype) constitutes a perilous resource acquisition campaign. Beneficial consortia, led by Christensenellaceae, synergize with highly activated secondary lipid metabolic axes (12,13-EpOME and LysoPC) and PXR receptor defenses driven by tryptophan derivatives (IPA), collectively injecting immense non-shivering thermogenic fuel to sustain baseline survival. However, this absolute prioritization of energy harvesting forces the host to decommission exceedingly costly intestinal immunosurveillance resources, resulting in severe hidden physiological costs characterized by the opportunistic expansion of *Klebsiella*. Once extreme stress surpasses the body's capacity to maintain this metabolic trade-off (the PP phenotype), it results in severe HPA axis decompensation, the accumulation of aberrant steroids (11-Epicortisol), and systemic low-grade inflammation driven by Fusobacterium overgrowth. This study not only overturns the traditional dogma equating "high physical adaptability" with "absolute health," precisely demarcating the threshold of human multi-optimality, but also pioneers highly promising translational targets for precision medical protection, postbiotic interventions, and endocrine stabilization in personnel operating in extreme environments.

Declarations

CRediT authorship contribution statement

Haonan Sun: Writing – original draft, Software, Methodology. Lixia Yu: Conceptualization. Jiafan Liang: Data curation. Jiahui Chen: Data curation. Guoping Zhao: Writing – review & editing, Resources. Zhanxin Yao: Investigation. Yanbo Wang: Supervision

Funding

No funding.

Declaration of competing interest

The authors declare that they have no known competing financial interests or personal relationships that could have appeared to influence the work reported in this paper.

Data availability

Data will be made available on request.

References

1. Akbuga-Schoen, T., Suzuki, T. A., Jakob, D., Vu, D. L., Waters, J. L., & Ley, R. E. (2024). The keystone gut species *Christensenella minuta* boosts gut microbial biomass and voluntary physical activity in mice. *mBio*, *15*(2). https://doi.org/10.1128/mbio.02836-23
2. Bäumler, A. J., & Sperandio, V. (2016). Interactions between the microbiota and pathogenic bacteria in the gut. *Nature*, *535*(7610), 85–93. https://doi.org/10.1038/nature18849
3. Bianchetti, G., De Maio, F., Abeltino, A., Serantoni, C., Riente, A., Santarelli, G., Sanguinetti, M., Delogu, G., Martinoli, R., Barbaresi, S., De Spirito, M., & Maulucci, G. (2023). Unraveling the gut microbiome-diet connection: Exploring the impact of digital precision and personalized nutrition on microbiota composition and host physiology. *Nutrients*, *15*(18), Article 3931. https://doi.org/10.3390/nu15183931
4. Boon, M. R., Bakker, L. E. H., Prehn, C., Adamski, J., Vosselman, M. J., Jazet, I. M., Arias-Bouda, L. M. P., van Lichtenbelt, W. D. M., van Dijk, K. W., Rensen, P. C. N., & Mook-Kanamori, D. O. (2017). LysoPC-acyl C16:0 is associated with brown adipose tissue activity in men. *Metabolomics*, *13*(5), Article 48. https://doi.org/10.1007/s11306-017-1185-z
5. Cain, D. W., & Cidlowski, J. A. (2017). Immune regulation by glucocorticoids. *Nature Reviews Immunology*, *17*(4), 233–247. https://doi.org/10.1038/nri.2017.1
6. Chen, Y. J., Xu, J. Y., & Chen, Y. (2021). Regulation of neurotransmitters by the gut microbiota and effects on cognition in neurological disorders. *Nutrients, 13*(6), Article 2099. https://doi.org/10.3390/nu13062099
7. do Amaral-Silva, L., da Silva, W. C., Gargaglioni, L. H., & Bícego, K. C. (2022). Metabolic trade-offs favor regulated hypothermia and inhibit fever in immune-challenged chicks. *Journal of Experimental Biology*, *225*(4), Article jeb243115. https://doi.org/10.1242/jeb.243115
8. Feng, X., Jia, M., Cai, M., Zhu, T., Yang, J. J., & Hashimoto, K. (2025). Central-peripheral neuroimmune dynamics in psychological stress and depression: Insights from current research. *Molecular Psychiatry*, *30*(10), 4881–4898. https://doi.org/10.1038/s41380-025-03085-y
9. Frankiensztajn, L. M., Elliott, E., & Koren, O. (2020). The microbiota and the hypothalamus-pituitary-adrenocortical (HPA) axis, implications for anxiety and stress disorders. *Current Opinion in Neurobiology*, *62*, 76–82. https://doi.org/10.1016/j.conb.2019.12.003
10. Hecht, A. L., Harling, L. C., Friedman, E. S., Tanes, C., Lee, J., Firrman, J., Hao, F., Tu, V., Liu, L., Patterson, A. D., Bittinger, K., Goulian, M., & Wu, G. D. (2024b). Dietary carbohydrates regulate intestinal colonization and dissemination of *Klebsiella pneumoniae*. *Journal of Clinical Investigation*, *134*(9), Article e174726. https://doi.org/10.1172/jci174726
11. Jiang, D., LaGory, E. L., Kenzelmann Brož, D., Bieging, K. T., Brady, C. A., Link, N., Abrams, J. M., Giaccia, A. J., & Attardi, L. D. (2015). Analysis of p53 transactivation domain mutants reveals Acad11 as a metabolic target important for p53 pro-survival function. *Cell Reports*, *10*(7), 1096–1109. https://doi.org/10.1016/j.celrep.2015.01.043
12. Jiang, S. S., Chen, Y. X., & Fang, J. Y. (2026). *Fusobacterium nucleatum: Ecology*, pathogenesis and clinical implications. *Nature Reviews Microbiology*, *24*(3), 197–214. https://doi.org/10.1038/s41579-

025-01237-z

13. Karl, J. P., Hatch, A. M., Arcidiacono, S. M., Pearce, S. C., Pantoja-Feliciano, I. G., Doherty, L. A., & Soares, J. W. (2018). Effects of psychological, environmental and physical stressors on the gut microbiota. *Frontiers in Microbiology, 9*, Article 2013. https://doi.org/10.3389/fmicb.2018.02013
14. Knezevic, E., Nenic, K., Milanovic, V., & Knezevic, N. N. (2023). The role of cortisol in chronic stress, neurodegenerative diseases, and psychological disorders. *Cells*, *12*(23), Article 2726. https://doi.org/10.3390/cells12232726
15. Lai, M., Zhou, W., Zou, W., Qiu, L., Liang, Z., Chen, W., Wang, Y., Guo, B., Zhao, C., Zhang, S., Lai, P., Hu, L., Liu, X., Jiang, Y., Chen, Y., Huang, M. J., Bai, X., & Zou, Z. (2025). Brown adipose tissue secretes OLFM4 to coordinate sensory and sympathetic innervation via Schwann cells. *Nature Communications*, *16*(1), 5206. https://doi.org/10.1038/s41467-025-60474-1
16. Li, J. J., Zhang, L., Wu, T., Li, Y. F., Zhou, X. J., & Ruan, Z. (2021). Indole-3-propionic acid improved the intestinal barrier by enhancing epithelial barrier and mucus barrier. *Journal of agricultural and food chemistry*, *69*(5), 1487–1495. https://doi.org/10.1021/acs.jafc.0c05205
17. Li, J. X., Tan, M. M., Hu, Z. G., Zhou, S. H., Liu, Z. B., Wang, C. X., Li, P., & Shan, F. B. (2026). The lactate-GPR81-PKA axis regulates exercise-induced central fatigue in male mice. *American Journal of Physiology-Regulatory, Integrative and Comparative Physiology*, *330*(2), R126-R135. https://doi.org/10.1152/ajpregu.00103.2025
18. Li, S. R., Liu, J. B., Yang, Q., Lyu, S., Han, Q. W., Fu, M. H., Du, Z. Y., Liu, X. T., & Zhang, T. (2025). Multi-omics analysis reveals the anti-fatigue mechanism of BCAA-enriched egg white peptides: The role of the gut-muscle axis. *Food & function*, *16*(5). https://doi.org/10.1039/d4fo04220d
19. Li, Z. Y., Liu, B., Li, S. H. J., King, C. G., Gitai, Z., & Wingreen, N. S. (2020). Modeling microbial metabolic trade-offs in a chemostat. *Plos Computational Biology*, *16*(8), Article e1008156. https://doi.org/10.1371/journal.pcbi.1008156
20. Lynes, M. D., Leiria, L. O., Lundh, M., Bartelt, A., Shamsi, F., Huang, T. L., Takahashi, H., Hirshman, M. F., Schlein, C., Lee, A., Baer, L. A., May, F. J., Gao, F., Narain, N. R., Chen, E. Y., Kiebish, M. A., Cypess, A. M., Blüher, M., Goodyear, L. J.,… Tseng, Y. H. (2017a). The cold-induced lipokine 12,13-diHOME promotes fatty acid transport into brown adipose tissue. *Nature Medicine*, *23*(5), 631–637. https://doi.org/10.1038/nm.4297
21. Montet, J., Montalban, E., Dexpert, S., Magne, E., Beau, C., Forestier, D., Ledaguenel, P., Gostner, J., Fuchs, D., Aouizerate, B., & Capuron, L. (2026). Inflammation-related alterations in tyrosine metabolism are associated with anhedonia and reduced motivation in obesity: Influence of early-life adversity. *Brain Behavior and Immunity*, *136*, Article 106547. https://doi.org/10.1016/j.bbi.2026.106547
22. Moreno-Navarrete, J. M., & Fernandez-Real, J. M. (2019). The gut microbiota modulates both browning of white adipose tissue and the activity of brown adipose tissue. *Reviews in Endocrine & Metabolic Disorders*, *20*(4), 387–397. https://doi.org/10.1007/s11154-019-09523-x

23. Nicholls, D. G., & Brand, M. D. (2023). A critical assessment of the role of creatine in brown adipose tissue thermogenesis. *Nature Metabolism*, *5*(1), 21–28. https://doi.org/10.1038/s42255-022-00718-2

24. Nieves, K. M., Flannigan, K. L., Hughes, E., Stephens, M., Thorne, A. J., Delanne-Cumenal, A., Strayer, K., Kola-Ilesanmi, D., Wickramasinghe, S., Mirzadzar, N., Baruta, G., McDonald, B., Cobo, E. R., Petri, B., Mani, S., & Hirota, S. A. (2025). Indole-3-propionic acid protects medium-diversity colitic mice via barrier enhancement preferentially over anti-inflammatory effects. *American Journal of Physiology-Gastrointestinal and Liver Physiology*, *328*(6), G696-G715. https://doi.org/10.1152/ajpgi.00256.2024

25. Polonio, C. M., & Quintana, F. J. (2024). Host-gut microbiota crosstalk predicts neuroinflammation. *Nature Microbiology*, *9*(9), 2204–2205. https://doi.org/10.1038/s41564-024-01790-y

26. Pontzer, H., Durazo-Arvizu, R., Dugas, L. R., Plange-Rhule, J., Bovet, P., Forrester, T. E., Lambert, E. V., Cooper, R. S., Schoeller, D. A., & Luke, A. (2016). Constrained total energy expenditure and metabolic adaptation to physical activity in adult humans. *Current Biology*, *26*(3), 410–417. https://doi.org/10.1016/j.cub.2015.12.046

27. Ridlon, J. M., Ikegawa, S., Alves, J. M. P., Zhou, B., Kobayashi, A., Iida, T., Mitamura, K., Tanabe, G., Serrano, M., De Guzman, A., Cooper, P., Buck, G. A., & Hylemon, P. B. (2013). *Clostridium scindens*: A human gut microbe with a high potential to convert glucocorticoids into androgens. *Journal of Lipid Research*, *54*(9), 2437–2449. https://doi.org/10.1194/jlr.M038869

28. Schoeler, M., & Caesar, R. (2019). Dietary lipids, gut microbiota and lipid metabolism. *Reviews in Endocrine & Metabolic Disorders*, *20*(4), 461–472. https://doi.org/10.1007/s11154-019-09512-0

29. Stanford, K. I., Lynes, M. D., Takahashi, H., Baer, L. A., Arts, P. J., May, F. J., Lehnig, A. C., Middelbeek, R. J. W., Richard, J. J., So, K., Chen, E. Y., Gao, F., Narain, N. R., Distefano, G., Shettigar, V. K., Hirshman, M. F., Ziolo, M. T., Kiebish, M. A., Tseng, Y. H.,… Goodyear, L. J. (2018). 12,13-diHOME: An exercise-induced lipokine that increases skeletal muscle fatty acid uptake. *Cell Metabolism*, *27*(5), 1111–1120. https://doi.org/10.1016/j.cmet.2018.03.020

30. Stephens, R. S., & Whitman, G. J. (2015). Postoperative Critical Care of the Adult Cardiac Surgical Patient. Part I: Routine Postoperative Care. *Critical Care Medicine*, *43*(7), 1477–1497. https://doi.org/10.1097/ccm.0000000000001059

31. van Wijck, K., Lenaerts, K., van Loon, L. J. C., Peters, W. H. M., Buurman, W. A., & Dejong, C. H. C. (2011). Exercise-induced splanchnic hypoperfusion results in gut dysfunction in healthy men. *PLOS ONE*, *6*(7), Article e22366. https://doi.org/10.1371/journal.pone.0022366

32. Vermeij, G. J., Grosberg, R. K., & Roopnarine, P. D. (2025). Energetics and evolutionary fitness. *Proceedings of the National Academy of Sciences of the United States of America*, *122*(21), Article e2423684122. https://doi.org/10.1073/pnas.2423684122

33. Venkatesh, M., Mukherjee, S., Wang, H. W., Li, H., Sun, K., Benechet, A. P., Qiu, Z. J., Maher, L., Redinbo, M. R., Phillips, R. S., Fleet, J. C., Kortagere, S., Mukherjee, P., Fasano, A., Le Ven, J., Nicholson, J. K., Dumas, M. E., Khanna, K. M., & Mani, S. (2014). Symbiotic Bacterial Metabolites

Regulate Gastrointestinal Barrier Function via the Xenobiotic Sensor PXR and Toll-like Receptor 4. *Immunity*, *41*(2), 296–310. https://doi.org/10.1016/j.immuni.2014.06.014

34. Wang, J., Cong, Y., Tang, B., Liu, J., & Pu, K. (2025). Integrative analysis of multi-omics data and gut microbiota composition reveals prognostic subtypes and predicts immunotherapy response in colorectal cancer using machine learning. *Scientific Reports*, *15*(1), Article 25268. https://doi.org/10.1038/s41598-025-08915-1
35. Waters, J. L., & Ley, R. E. (2019). The human gut bacteria Christensenellaceae are widespread, heritable, and associated with health. *BMC Biol*, *17*(1), 83. https://doi.org/10.1186/s12915-019-0699-4
36. Wegierska, A. E., Charitos, I. A., Topi, S., Potenza, M. A., Montagnani, M., & Santacroce, L. (2022). The connection between physical exercise and gut microbiota: Implications for competitive sports athletes. *Sports Medicine*, *52*(10), 2355–2369. https://doi.org/10.1007/s40279-022-01696-x
37. Ying, Z. X., Tramper, N., Zhou, E. C., Boon, M. R., Rensen, P. C. N., & Kooijman, S. (2023). Role of thermogenic adipose tissue in lipid metabolism and atherosclerotic cardiovascular disease: Lessons from studies in mice and humans. *Cardiovascular Research*, *119*(4), 905–918. https://doi.org/10.1093/cvr/cvac131
38. Zheng, D. P., Liwinski, T., & Elinav, E. (2020). Interaction between microbiota and immunity in health and disease. *Cell Research*, *30*(6), 492–506. https://doi.org/10.1038/s41422-020-0332-7

Figures

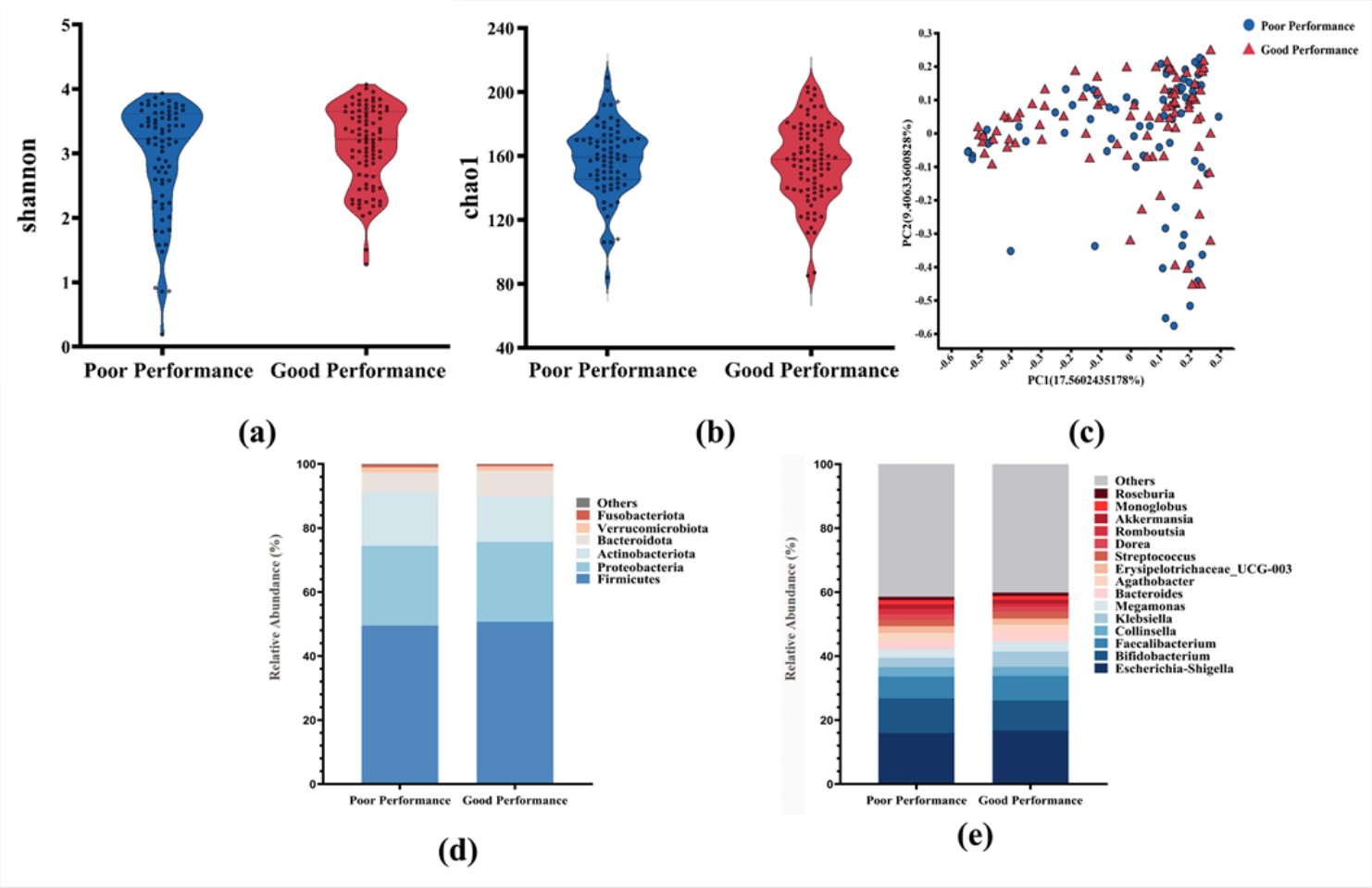


Figure 1

Gut microbiota diversity and community structure across different physical performance phenotypes. (a) Alpha diversity estimated by the Shannon index, reflecting community evenness and diversity. (b) Alpha diversity estimated by the Chao1 index, reflecting species richness. (c) Principal Coordinate Analysis (PCoA) plot based on Bray-Curtis dissimilarity, illustrating the beta diversity and partial clustering separation between the two cohorts. GP: Good Performance group (red); PP: Poor Performance group (blue). (d) Relative abundance of the dominant bacterial taxa at the phylum level in the Poor Performance (PP) and Good Performance (GP) groups. (e) Relative abundance of the dominant bacterial taxa at the genus level across the two cohorts. Taxa with an average relative abundance of less than 1% are grouped into "Others".



Figure 2

Identification of key differential microbial biomarkers between extreme physical performance phenotypes using Linear Discriminant Analysis Effect Size (LEfSe) analysis. (a) Cladogram illustrating the phylogenetic distribution and hierarchical relationship of the differentially abundant microbial taxa. The size of each node is proportional to the relative abundance of the taxa. (b) Histogram of Linear Discriminant Analysis (LDA) scores evaluating the effect size of the differential biomarkers. Taxa enriched in the Good Performance (GP) group are indicated in red, while those enriched in the Poor Performance (PP) group are indicated in blue. Only taxa meeting the significant LDA threshold (≥3) are shown.

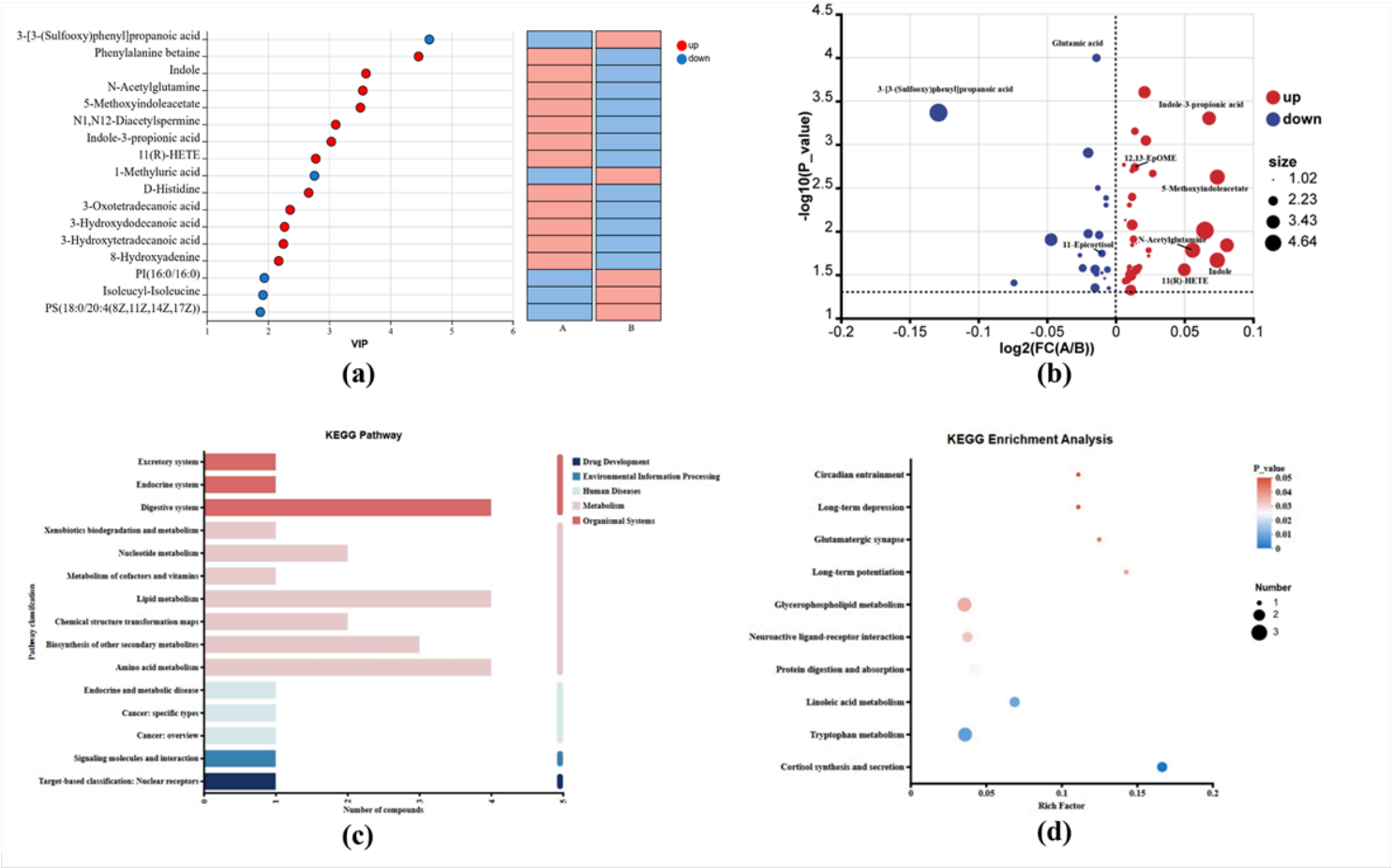


Figure 3

Untargeted metabolomic profiling and functional pathway enrichment analysis. (a) VIP score plot identifying the top distinct metabolites driving the separation between the Good Performance (A) and Poor Performance (B) groups. Red dots indicate upregulated metabolites, while blue dots indicate downregulated metabolites in the respective comparisons. (b) Volcano plot illustrating the comprehensive distribution of differential metabolites. Each point represents a detected feature; red points indicate significantly upregulated metabolites, and blue points indicate significantly downregulated metabolites (fold change and *p*-value thresholds applied). (c) Bar chart of KEGG pathway classification, categorizing the identified differential metabolites into functional systems such as metabolism, organismal systems, and environmental information processing. (d) Bubble chart of KEGG pathway enrichment analysis, highlighting the top dysregulated metabolic pathways. The size of the bubble corresponds to the number of enriched metabolites within the pathway, and the color gradient represents the significance (*p*-value).

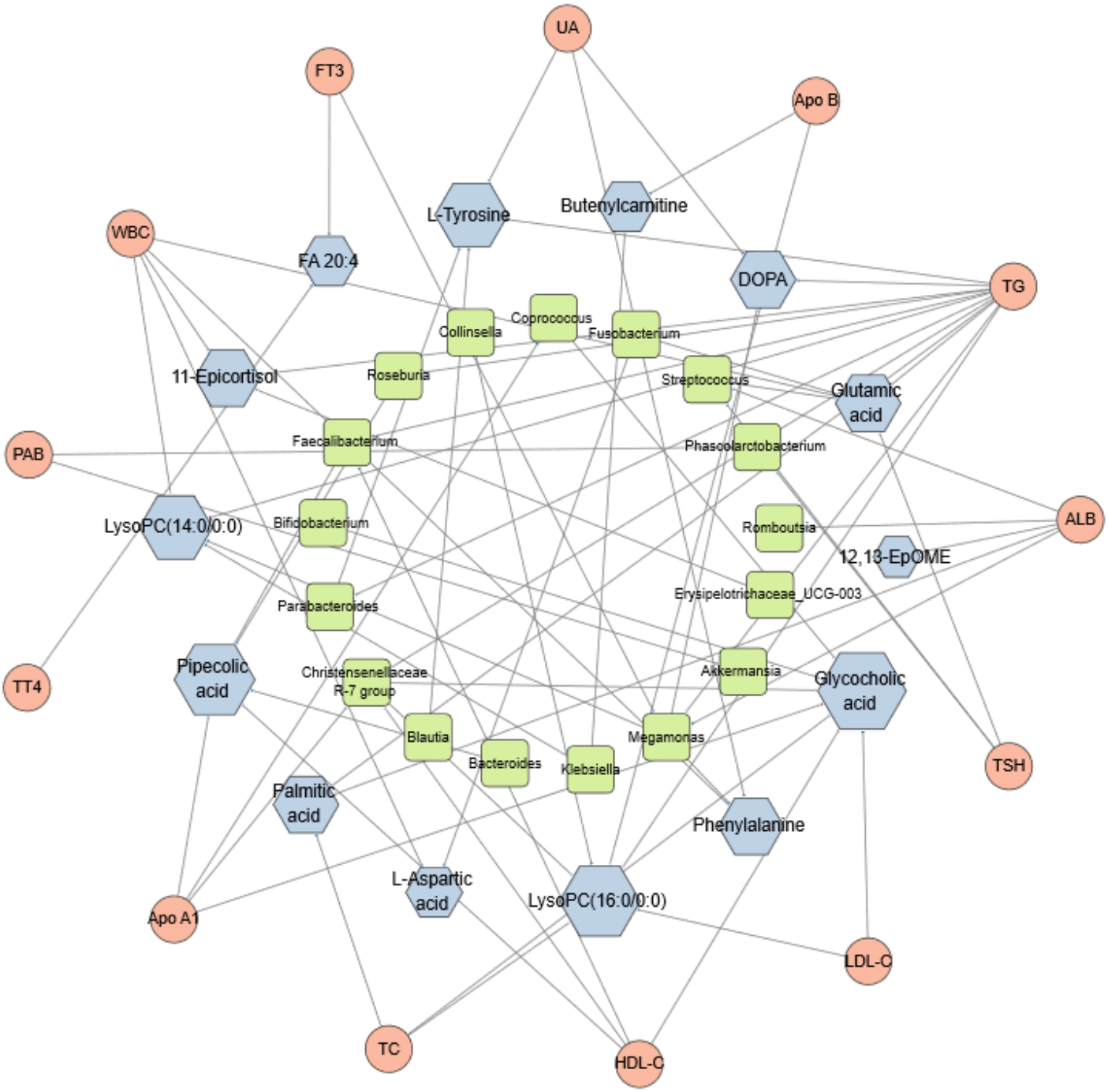


Figure 4

Trans-kingdom multi-omics interaction network integrating gut microbiota, fecal metabolome, and clinical phenotypes. The network was constructed based on Spearman rank correlation analysis. Only robust interaction edges satisfying an FDR-adjusted $q < 0.05$ and an absolute correlation coefficient $|r| \geq 0.20$ were retained. Green squares represent differential bacterial genera, blue hexagons denote key fecal metabolites, and red circles indicate clinical blood biochemical indices.